J Solid State Electrochem (2013) 17:1201–1206
DOI 10.1007/s10008-012-1980-4

ORIGINAL PAPER

Morphology-controllable synthesis of $LiMn_2O_4$ particles as cathode materials of lithium batteries

Xingde Xiang · Zhao Fu · Weishan Li

Received: 3 October 2012 / Revised: 8 December 2012 / Accepted: 14 December 2012 / Published online: 9 January 2013

Abstract We reported a new method for the preparation of morphology-controllable $LiMn_2O_4$ particles. In this method, dimension-different MnO_2 nanowires synthesized hydrothermally by adjusting the reaction temperature were used as the precursor. The morphology and structure of the resulting products were characterized with scanning electron microscope and X-ray diffraction, and the performances of the prepared $LiMn_2O_4$ samples as cathode material of lithium batteries were investigated by cyclic voltammetry and galvanostatic charge/discharge test. The results indicate that the morphology of $LiMn_2O_4$ transforms from tridimensional particle (TP) to unidimensional rod (UR) through quadrate lamina (QL) with increasing the diameter and length of MnO_2 nanowires. Although the cyclic stabilities of $LiMn_2O_4$-TP, $LiMn_2O_4$-QL, and $LiMn_2O_4$-UR are very close (the 0.1 C capacity after 50 cycles is 101, 93, and 99 mAh g^{-1} at 25 °C, and 84, 78, and 82 mAh g^{-1} at 50 °C, respectively), $LiMn_2O_4$-QL delivers much higher rate capacity (about 70 mAh g^{-1} at 5 C and 30 mAh g^{-1} at 10 C) than $LiMn_2O_4$-TP and $LiMn_2O_4$-UR (about 20 mAh g^{-1} at 5 C, 3 mAh g^{-1} at 10 C, 25 mAh g^{-1} at 5 C, and 3 mAh g^{-1} at 10 C).

X. Xiang · Z. Fu · W. Li
School of Chemistry and Environment, South China Normal University, Guangzhou 510006, China

X. Xiang · W. Li
School of Materials Science and Engineering, South China University of Technology, Guangzhou 510640, China

W. Li
Key Laboratory of Electrochemical Technology on Energy Storage and Power Generation of Guangdong Higher Education Institutes, South China Normal University, Guangzhou 510006, China

W. Li (✉)
Engineering Research Center of Materials and Technology for Electrochemical Energy Storage (Ministry of Education), South China Normal University, Guangzhou 510006, China
e-mail: liwsh@scnu.edu.cn

Keywords Manganese dioxide · Spinel lithium manganese oxide · Cathode · Lithium batteries

Introduction

Lithium ion battery has been attracting much attention for its application in the field of electric vehicles (EV) or hybrid electric vehicles (HEV) due to its high energy density and environmental benignity [1, 2]. Cost and rate performance are the main concerns for the application of lithium ion battery in EV/HEV [1]. Compared to other commercial cathode materials of lithium ion battery, such as $LiCoO_2$ and $LiCo_{1/3}Ni_{1/3}Mn_{1/3}O_2$, spinel $LiMn_2O_4$ is the most competitive for EV/HEV because of its rich resource and easy preparation [1, 3–7]. However, the rate capability of $LiMn_2O_4$ needs to be improved for its application in EV/HEV.

The rate capability of $LiMn_2O_4$ is determined by the rapid insertion/desertion of lithium ions in $LiMn_2O_4$ matrix, which is seriously influenced by the particle size and morphology. Small particles can supply short pathway and large area for diffusion of lithium ions and thus favors delivering the rate capacity [8–10]. It has been found that the rate capacity of $LiMn_2O_4$ can be improved by designing nanoparticle size [11–15]. Kim et al. [11] synthesized $LiMn_2O_4$ nanorods growing in <110> that could deliver much higher capacity than the commercial sample. Lee et al. [12] reported that ultrathin $LiMn_2O_4$ nanowires delivered 102 mAh g^{-1} at 10 C and 62 mAh g^{-1} at 30 C with good capacity retention and structural stability in the region of 3.1~4.3 V. Similar result was obtained by Hosono et al. [13]. Luo et al. fabricated a series of $LiMn_2O_4$ with high rate performance, such as $LiMn_2O_4$ nanothorn microspheres, $LiMn_2O_4$ hollow nanospheres, and ordered mesoporous $LiMn_2O_4$ [14]. However, the reduced particle size of $LiMn_2O_4$ increases its contact area with electrolyte, which might lead to severe decomposition of electrolyte and the dissolution of manganese in $LiMn_2O_4$ [16, 17].

With the aim to obtain $LiMn_2O_4$ that has less surface area but exhibits good rate performance, dimension-different MnO_2 nanowires were synthesized hydrothermally in this work by adjusting the reaction temperature and used as the precursors to induce the morphology-controllable synthesis of $LiMn_2O_4$ particles. A comparative study of resulting $LiMn_2O_4$ samples with different morphology was performed by using X-ray diffraction, scanning electron microscope, cyclic voltammetry, and charge/discharge test.

Experimental

Preparation

MnO_2 precursor was firstly synthesized by a hydrothermal approach as reported by Wang et al. [18] and Kim et al. [11]. Specially, 10 g of manganese acetate ($Mn(CH_3COO)_2 \cdot 4H_2O$) and 9.4 g of ammonium persulfate ($(NH_4)_2S_2O_8$) were dissolved into 80 ml of distilled water under magnetic stirring to form a homogeneous solution. The resulting solution was transferred into 100 ml of Teflon-lined stainless autoclave and then heated at 120 °C for 12 h. After being cooled to room temperature, the product was filtrated, washed, and air-dried at 100 °C for 10 h. This product was denoted as MnO_2-120. Two other samples were also prepared in the same process except for the hydrothermal temperature, 160 °C for MnO_2-160 and 200 °C for MnO_2-200.

$LiMn_2O_4$ was prepared as follows. Specially, MnO_2 nanowires and LiOH with the molar ratio of 2:1.05 were added into 60-ml of distilled water in order under vigorous stirring, and then the slurry was evaporated at 80 °C. The dried powder was heated to 750 °C with the heating rate of 3 °C min^{-1} and kept at 750 °C for 12 h. This morphology-controllable synthesis process of $LiMn_2O_4$ can be described as Scheme 1.

Characterization

Morphology of the sample was observed by scanning electron microscope (JSM-6380, Japan); X-ray diffraction was performed on a Rigaku D/max 2200 vpc diffractometer operated at 30 kV and 20 mA with Cu K_α radiation. Galvanostatic charge/discharge tests were carried out on a LAND cell test (Land CT 2001A) system.

Electrochemical measurements

The electrode for electrochemical measurements was prepared as follows: 80 wt% active material ($LiMn_2O_4$), 10 wt% conductive material (acetylene black), and 10 wt% polyvinylidene fluoride binder (PVDF) were mixed in *N*-methyl-2-pyrrolidone. The resulting slurry was coated on an aluminum sheet and dried. The coated sheet was cut into pieces of 1 cm × 1 cm.

The electrochemical measurements were carried out on a CR2032-type coin cell with the lithium foil as the counter electrode. The electrolyte was 1 mol L^{-1} $LiPF_6$ dissolved in a mixture of ethylene carbonate and dimethyl carbonate (1:1 by volume). The separator of cell was Celgard 2400. The coin cells were assembled in an Ar-filled glove box (Mikrouna, Super 1220/750/900). The assembled cells were aged overnight before testing.

Results and discussion

Morphology and structure

MnO_2 is usually used as the precursor to prepare $LiMn_2O_4$ with high performance, and it has been known that morphology of MnO_2 determines to some extent the morphology and performance of resultant $LiMn_2O_4$. Based on this knowledge, we try to prepare $LiMn_2O_4$ with different morphologies by adjusting the dimension of MnO_2 precursor. Figure 1 presents the SEM images of the precursors and corresponding products. It can be seen from Fig. 1a, b, c that the resulting MnO_2 precursors are nanowires, and their size is influenced by hydrothermal temperature, with a tendency of increased MnO_2 grain size with elevating temperature. MnO_2-120, MnO_2-160, and MnO_2-200 are 25, 45, and 75 nm in diameter and 0.5, 1.0, and 1.5 μm in length, respectively. As seen from Fig. 1d–i, the morphology of

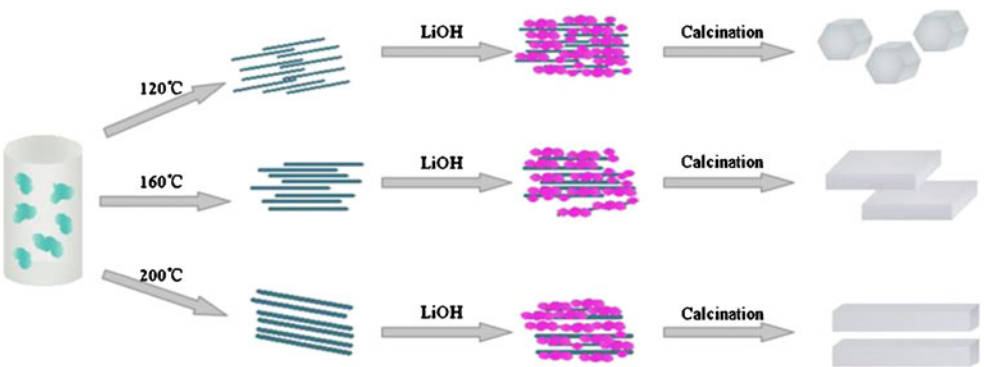

Scheme 1 Schematic morphology-controllable synthesis process of $LiMn_2O_4$

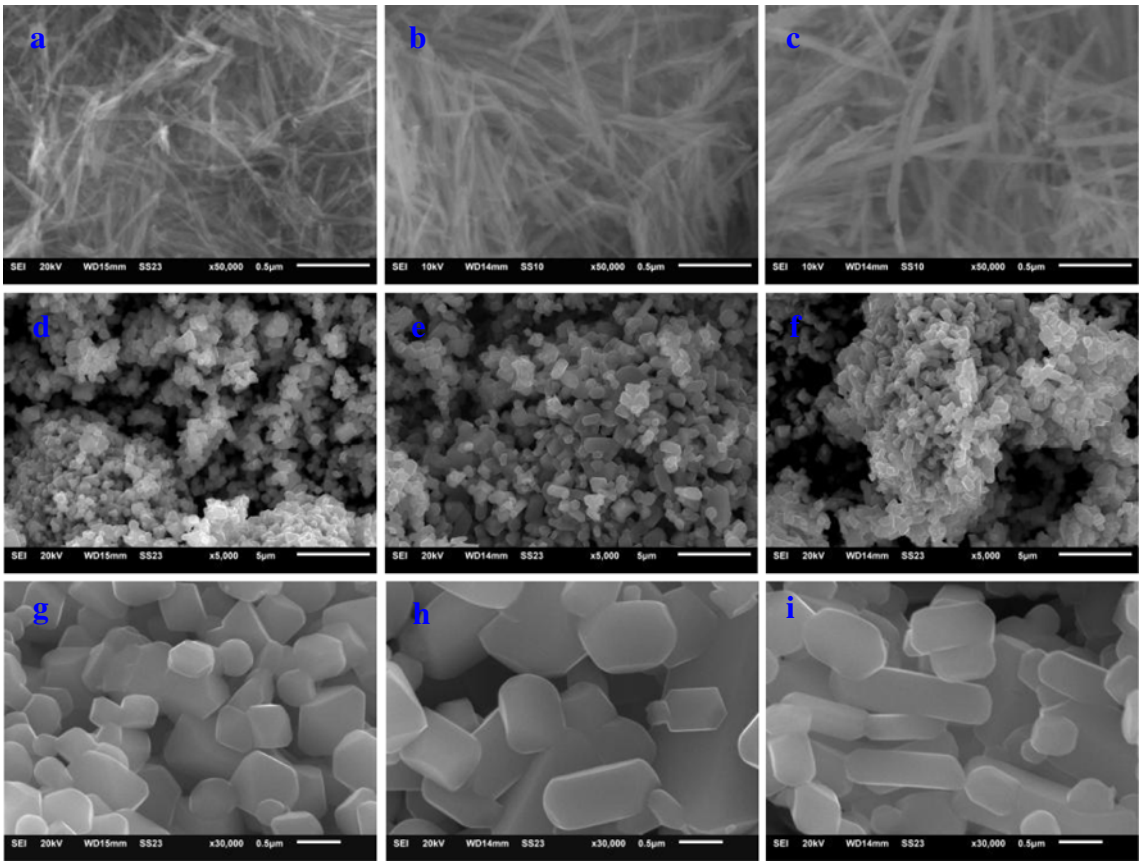

Fig. 1 SEM images of precursors, MnO_2-120 (**a**), MnO_2-160 (**b**), MnO_2-200 (**c**), and corresponding products, $LiMn_2O_4$-TP (**d**, **g**), $LiMn_2O_4$-QL (**e**, **h**), and $LiMn_2O_4$-UR (**f**, **i**)

the resulting $LiMn_2O_4$ from MnO_2-120, MnO_2-160, and MnO_2-200 is tridimensional particle (TP), quadrate lamina (QL), and unidimensional rod (UR), respectively, indicating that the morphology of $LiMn_2O_4$ can be controllable with structure-defined MnO_2 precursor. Therefore, the resulting products are denoted as $LiMn_2O_4$-TP, $LiMn_2O_4$-QL, and $LiMn_2O_4$-UR, respectively. The formation mechanism of the different morphology can be explained as follows. MnO_2 decomposes to Mn_3O_4 and O_2 before lithium intercalation, and Mn_3O_4 expands after lithium intercalation. In

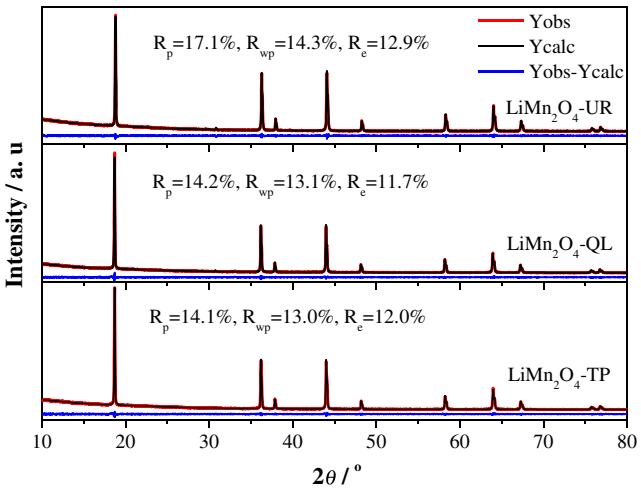

Fig. 2 XRD patterns of the prepared samples, $LiMn_2O_4$-TP, $LiMn_2O_4$-QL, and $LiMn_2O_4$-UR

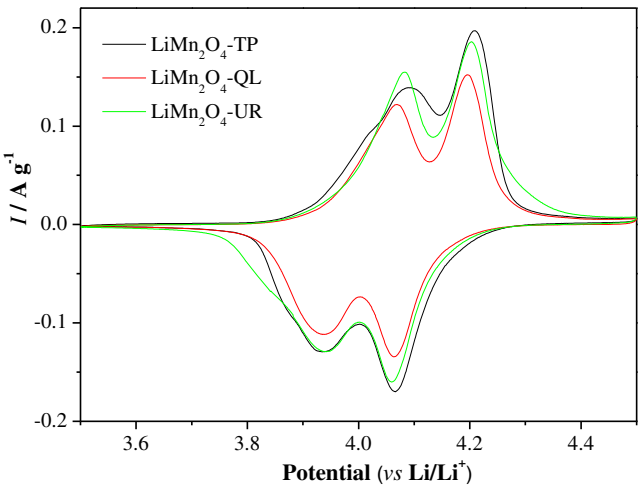

Fig. 3 Cyclic voltammograms of $LiMn_2O_4$-TP, $LiMn_2O_4$-QL, and $LiMn_2O_4$-UR with a scanning rate of 0.1 mVs^{-1}

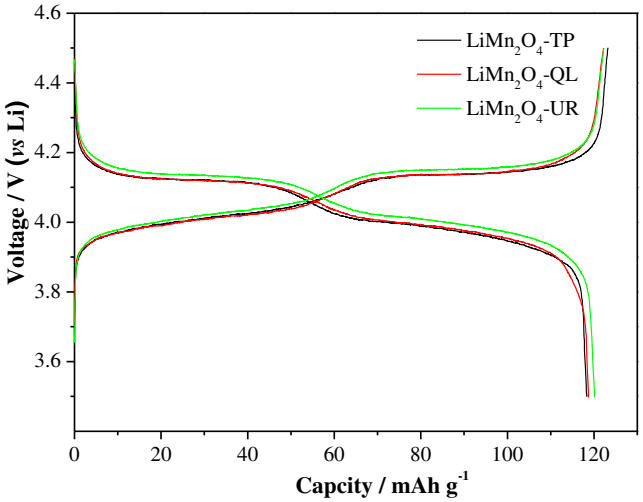

Fig. 4 Charge/discharge curves of $LiMn_2O_4$-TP, $LiMn_2O_4$-QL, and $LiMn_2O_4$-UR at 0.1 C

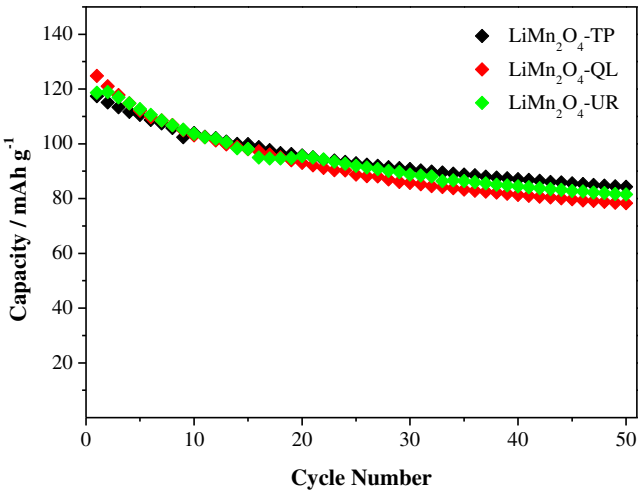

Fig. 6 Cyclic stability of $LiMn_2O_4$-TP, $LiMn_2O_4$-QL, and $LiMn_2O_4$-UR at 50 °C (0.1 C, 3.5–4.5 V)

the process of decomposition and expansion, MnO_2 nanowires with smaller diameter are easily destroyed, thus inducing the formation of $LiMn_2O_4$ with tridimensional particles. With increasing diameter, the precursor MnO_2 keeps its nanowire structure, forming $LiMn_2O_4$ particles with their size similar to rods.

The crystal structure of the resulting $LiMn_2O_4$ was determined by XRD. The XRD patterns of three products are showed in Fig. 2. It can be seen from Fig. 2 that three samples exhibit a typical feature of spinel structure with *Fd3m* space group [19, 20]. There are ten sharp peaks located at 18.6°, 36.2°, 37.9°, 44.0°, 48.2°, 58.2°, 64.0°, 67.3°, 75.8°, and 76.8°, corresponding to (111), (311), (222), (400), (331), (511), (440), (531), (533), and (622) planes of $LiMn_2O_4$, respectively. To obtain the lattice parameters of the three $LiMn_2O_4$ samples, XRD refinement was performed with FullProf software [21], and fitted results are showed in Fig. 2. The lattice parameter of three samples is similar; 8.231 Å for $LiMn_2O_4$-TP, 8.236 Å for $LiMn_2O_4$-QL, and 8.239 Å for $LiMn_2O_4$-UR. It has been reported that lattice parameter is tightly associated with Mn^{3+}/Mn^{4+} ratio in $LiMn_2O_4$, which is important to the cyclic stability of $LiMn_2O_4$, especially at elevated temperature [22]. The similar lattice parameter suggests that three samples have similar cyclic performance, which can be confirmed by Figs. 5 and 6.

Electrochemical behavior

The electrochemical reversibility of three $LiMn_2O_4$ samples were investigated by cyclic voltammetry, and Fig. 3 shows the cyclic voltammograms of $LiMn_2O_4$-TP, $LiMn_2O_4$-QL, and $LiMn_2O_4$-UR at a scanning rate of 0.1 mVs^{-1}. Two pairs of redox peaks can be clearly identified at around 4.0 and 4.1 V. As we know, the ratio of the cathodic peak current to anodic

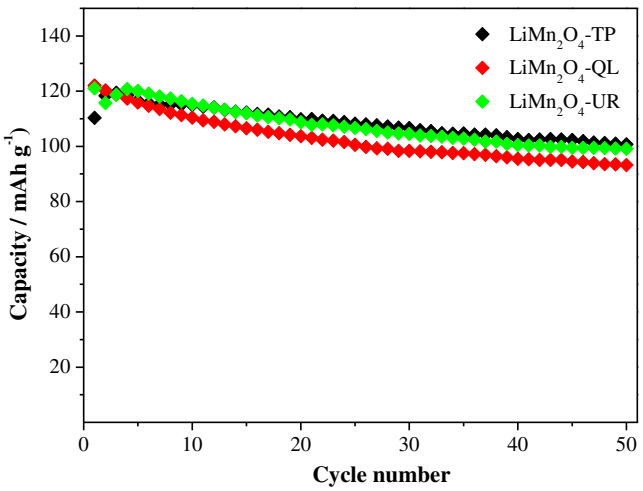

Fig. 5 Cyclic stability of $LiMn_2O_4$-TP, $LiMn_2O_4$-QL, and $LiMn_2O_4$-UR at 25 °C (0.1 C, 3.5–4.5 V)

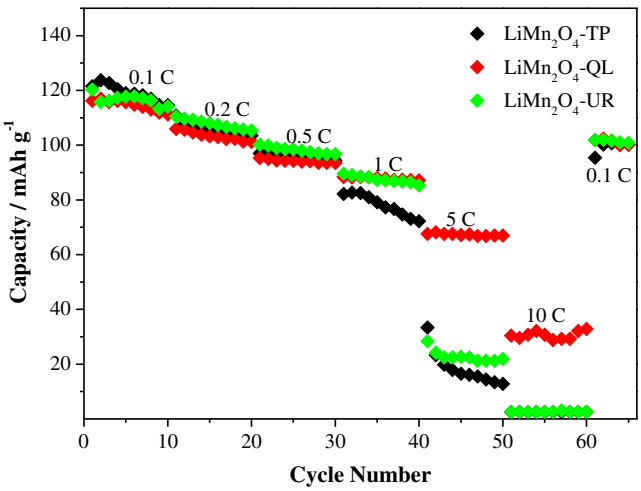

Fig. 7 Rate capability of $LiMn_2O_4$-TP, $LiMn_2O_4$-QL, and $LiMn_2O_4$-UR at 25 °C

peak current (I_{pc}/I_{pa}) and the difference between cathodic peak potential and anodic peak potential ($E_{pc} - E_{pa}$) are the key indicatives of electrochemical reversibility. For $LiMn_2O_4$-TP, $LiMn_2O_4$-QL, and $LiMn_2O_4$-UR, the I_{pc}/I_{pa} values at 4.0 and 4.1 V are 0.93 and 0.86, 0.92 and 0.88, and 0.83 and 0.86, and the ($E_{pc} - E_{pa}$) values are 161 and 141 mV, 134 and 132 mV, and 145 and 144 mV, respectively. It is evident that $LiMn_2O_4$-QL has the minimum value of $E_{pc} - E_{pa}$ and the closest value of I_{pc}/I_p to 1, implying that $LiMn_2O_4$-QL has the best electrochemical reversibility. The difference in electrochemical reversibility among three samples should be related to their different morphology.

The charge/discharge curves of $LiMn_2O_4$-TP, $LiMn_2O_4$-QL, and $LiMn_2O_4$-UR are given in Fig. 4. There are two plateaus located at 4.0 and 4.1 V, corresponding to the two pairs of redox peaks of Fig. 3, which reflect the two steps for the insertion/desertion of lithium ions in $LiMn_2O_4$ matrix [23, 24]. In the first step, lithium ions occupy half of available tetrahedral sites (8a) in spinel $LiMn_2O_4$ structure, corresponding to $Li_xMn_2O_4$ ($0<x<0.5$) in lithium-defected state. In the second step, lithium ions further occupy the remaining empty 8a sites, assigned to $Li_xMn_2O_4$ ($0.5\leq x\leq 1$) in lithium-rich state. The repulsive interaction of lithium ions in lithium-rich state is much stronger than that in lithium-defected state, causing larger polarization for insertion/desertion of lithium ions in the second step [25]. It seems that no significant difference in charge/discharge performance can be identified among three samples at thus low rate (0.1 C).

One of problems for the use of $LiMn_2O_4$ as cathode of lithium battery is capacity decay with cycling, which results from the destruction of spinel structure due to the continuous expansion and contraction with the insertion and desertion of lithium ions [26]. The cyclic performance of our prepared $LiMn_2O_4$ samples was investigated at 0.1 C under 25 and 50 °C between 3.5 and 4.5 V. Figures 5 and 6 present the capacity variation of the samples with cycling. The 0.1 C capacity of $LiMn_2O_4$-TP, $LiMn_2O_4$-QL, and $LiMn_2O_4$-UR at 50th cycle is 101, 93, and 99 mAh g^{-1} at 25 °C, and 84, 78, and 82 mAh g^{-1} at 50 °C, respectively. The capacity decay can be observed for all the samples and becomes worse at elevated temperature that causes easily the severe dissolution of manganese and decomposition of electrolyte [17, 27]. It can be noted that there is no significant difference in the cyclic stability among three samples.

Interestingly, although three samples have similar low rate capacity and cyclic stability, their high rate performance is different. Figure 7 presents the capacity variation of three samples with rates. The significant difference in capacity can be observed at higher rates (5 and 10 C). The discharge capacity of $LiMn_2O_4$-TP at high rate is instable, decreasing from 82 to 72 mAh g^{-1} in 10 cycles at 1 C, and from 33 to 13 mAh g^{-1} in 10 cycles at 5 C. $LiMn_2O_4$-UR shows better stability at higher rate but still delivers low rate capacity; 90 mAh g^{-1} at first cycle and 85 mAh g^{-1}at tenth cycle for 1C, 28 mAh g^{-1}at first cycle and 22 mAh g^{-1} at tenth cycle for 5 C. Differently, $LiMn_2O_4$-QL shows good stability and rate performance; 88 mAh g^{-1} at first cycle and 87 mAh g^{-1} at tenth cycle for 1 C, 68 mAh g^{-1} at first cycle and 67 mAh g^{-1} at tenth cycle for 5 C. When the rate rises to 10 C, the capacities of $LiMn_2O_4$-TP and $LiMn_2O_4$-UR are negligible (about 3 mAh g^{-1}), but the capacity of $LiMn_2O_4$-QL retains about 30 mAh g^{-1}, indicative of the superior rate performance of $LiMn_2O_4$-QL. The superior rate performance of $LiMn_2O_4$-QL should be related to its good electrochemical reversibility.

Conclusions

Morphology-controllable synthesis of $LiMn_2O_4$ can be realized by using MnO_2 nanowires with different dimensions as the precursor. The MnO_2 nanowires can be easily obtained by adjusting the reaction temperature in a hydrothermal approach. The cyclic stability of the prepared $LiMn_2O_4$ samples with tridimensional particle, quadrate lamina, and unidimensional rod are similar at low rate (0.1 C), but $LiMn_2O_4$ with quadrate lamina exhibits better cyclic stability and discharge capacity at high rate (>1 C). The better rate performance of $LiMn_2O_4$ with quadrate lamina can be attributed to its better electrochemical reversibility.

Acknowledgments The authors are highly grateful for the financial support from the joint project of National Natural Science Foundation of China and Natural Science Foundation of Guangdong Province (Grant No. U1134002), the National Natural Science Foundation (Grant No. 21273084), the Natural Science Fund of Guangdong Province (Grant No. 10351063101000001), and the key project of Science and Technology in Guangdong Province (Grant No. 2012A010702003).

References

1. Park OK, Cho Y, Lee S, Yoo HC, Song HK, Cho J (2011) Energy Environ Sci 4:1621–1633
2. Luo JY, Wang YG, Xiong HM, Xia YY (2007) Chem Mater 19:4791–4795
3. Xiong LL, Xu YL, Zhang C, Zhang ZW, Li JB (2011) J Solid State Electrochem 15:1263–1269
4. Qing CB, Bai Y, Yang JM, Zhang WF (2011) Electrochim Acta 56:6612–6618
5. Wang YP, Wang XY, Yang SY, Shu HB, Wei QL, Wu Q, Bai YS, Hu BA (2012) J Solid State Electrochem 16:2913–2920
6. Tan CL, Zhou HJ, Li WS, Lu DS, Hou XH, Xu MQ, Huang QM (2008) J Power Sources 184:408–413
7. Zeng RH, Li WS, Lu DS, Huang QM (2007) J Power Sources 174:592–597
8. Okubo M, Mizuno Y, Yamada H, Kim J, Hosono E, Zhou HS, Kudo T, Honma I (2010) ACS Nano 4:741–752
9. Lu CH, Lin SW (2001) J Power Sources 97–98:458–460
10. Crain D, Zheng JP, Sulyma C, Goia C, Goia D, Roy D (2012) J Solid State Electrochem 16:2605–2615

11. Kim DK, Muralidharan P, Lee HW, Ruffo R, Yang Y, Chan CK, Peng H, Huggins RA, Cui Y (2008) Nano Lett 8:3948–3952
12. Lee HW, Muralidharan P, Ruffo R, Mari CM, Cui Y, Kim DK (2010) Nano Lett 10:3852–3856
13. Hosono E, Kudo T, Honma I, Matsuda H, Zhou HS (2009) Nano Lett 9:1045–1051
14. Luo JY, Xiong HM, Xia YY (2008) J Phys Chem C 112:12051–12057
15. Bao SJ, Li CM, Li HL, Luong JHT (2007) J Power Sources 164:885–889
16. Matsuda K, Taniguchi I (2004) J Power Sources 132:156–160
17. Amatucci G, Pasquier AD, Blyr A, Zheng T, Tarascon JM (1999) Electrochim Acta 45:255–271
18. Wang X, Li YD (2002) J Am Chem Soc 124:2880–2881
19. Jayalakshmi M, Rao MM, Scholz F (2003) Langmuir 19:8403–8408
20. Shaju KM, Bruce PG (2008) Chem Mater 20:5557–5562
21. Rodriguez-Carvajal J (1990) In: Satellite meeting on powder diffraction of the XV Congress of the IUCr 127; International Union of Crystallography: Toulouse, France
22. Chung H-T, Myung S-T, Cho T-H, Son J-T (2001) J Power Sources 97–98:454–457
23. Liu W, Farrington GC, Chaput F, Dunn B (1996) J Electrochem Soc 143:879–884
24. Liu W, Wowal K, Farrington GC (1998) J Electrochem Soc 145:459–465
25. Lu DS, Li WS, Zuo XX, Yuan ZZ, Huang QM (2007) J Phys Chem C 111:12067–12074
26. Song MY, Ahn DS, Park HR (1999) J Power Sources 83:57–60
27. Chung KY, Lee HS, Yoon WS, McBreen J, Yang XQ (2006) J Electrochem Soc 153:A774–A780